The final published article is available at Elsevier as: A. Léger, L. Weber and A. Mortensen, "Influence of the wetting angle on capillary forces in pressure infiltration", *Acta Materialia*, Vol. 91 (2015) pp. 57-69 doi:10.1016/j.actamat.2015.03.002.

Influence of the wetting angle on capillary forces in pressure infiltration

Authors: *Alain Léger[a*], Ludger Weber[a] and Andreas Mortensen[a]*

Affiliations:

[a]Laboratory of Mechanical Metallurgy, EPFL, Station 12, CH-1015 Lausanne, Switzerland.

**Correspondence to: alain.leger@alumni.epfl.ch, Present address: Kugler Bimetal SA, Chemin du Château-Bloch 17, Case postale 26, CH–1219, Le Lignon/Genève, Switzerland.*

Phone number: +41 79 756 70 42

ludger.weber@epfl.ch; phone number: +41 21 693 29 34

andreas.mortensen@epfl.ch, phone number: +41 21 693 29 12

Abstract

This work probes the influence of wetting on pressure infiltration. Pressure/saturation curves for the infiltration of packed F-1000 angular alumina particle preforms by liquid Cu-Al and Sn-Al alloys are measured using an instrumented high-temperature pressure infiltration apparatus. These are ceramic-metal systems in which the contact angle is documented to vary significantly with alloying, from non-wetting to wetting conditions. We show that adding Al to Sn or to Cu modifies the early percolation-dominated phases of infiltration and also the later, pore geometry dominated, phase of the infiltration process. Changes in contact angle brought by alloying cause the saturation/pressure curves to shift, yet for all systems of this work the curves remain entirely in the range of positive pressures, despite a transition to contact angles below 90°. Combining measured pressures for infiltration at fixed saturation with relevant sessile drop experiment data from the literature shows that for, the range of conditions explored here, the infiltration pressures required are proportional, not to the work of immersion, but to a linear function thereof. This result agrees qualitatively with prior work in the literature on the infiltration of non-metallic liquids in porous media, and provides a master curve by means of which saturation curves and sessile drop data can be reconciled for this particular packed ceramic particle preform.

The final published article is available at Elsevier as: A. Léger, L. Weber and A. Mortensen, "Influence of the wetting angle on capillary forces in pressure infiltration", *Acta Materialia*, Vol. 91 (2015) pp. 57-69 doi:10.1016/j.actamat.2015.03.002.

Keywords: liquid metal infiltration, invasion percolation, work of immersion, wetting angle, aluminium, alumina

Introduction

Pressure infiltration is one of the best ways of combining a metal with a refractory phase to produce composites of high microstructural quality, rapidly and to net or near-net shape [1-6]. In metal infiltration capillary forces are high and when the preform is not metallic these generally tend to oppose entry of the metal into preform pores. Quantifying capillarity in infiltration processing is thus important; this can be done as in soil science or reservoir engineering, by measuring saturation curves, also known as drainage/imbibition curves [7-8]. Those curves are, in the present context, plots of the volume fraction of metal that has invaded pores of the evacuated porous refractory "preform" versus the pressure difference between the metal and the empty preform pores, as measured under conditions of static capillary equilibrium, meaning once flow of the metal into or out of the preform has stopped.

The saturation S corresponding to the non-wetting fluid (here the metal) is defined by:

$$S \equiv \frac{V_{\mathrm{m}}}{1-V_{\mathrm{r}}} \qquad (1)$$

where V_{m} and V_{r} are the volume fractions of metal and reinforcement in the composite, respectively. A saturation curve plots S versus the pressure difference P between the metal as it invades preform pores and the atmosphere present in uninfiltrated pores. If the preform was initially evacuated (as is the case in present experiments), then P is simply the metal pressure, *i.e.* the sum of applied pressure and metallostatic pressure. In practice, the latter is much smaller than the former and is hence generally neglected.

Measuring saturation curves in the context of metallurgical processing is challenging because both the temperatures and the pressures involved tend to be high (typical orders of magnitude are 1000 °C and 100 atmospheres). Methods have nonetheless been developed to enable this [9-

The final published article is available at Elsevier as: A. Léger, L. Weber and A. Mortensen, "Influence of the wetting angle on capillary forces in pressure infiltration", *Acta Materialia*, Vol. 91 (2015) pp. 57-69 doi:10.1016/j.actamat.2015.03.002.

17]. Here we use an infiltration apparatus capable of measuring with high precision the changes in metal free surface position during high pressure and high temperature infiltration of porous preforms. This apparatus can trace an entire saturation curve in a single experiment at pressures and temperatures characteristic of metallurgical processes; the apparatus and associated methods are described in Refs. [13, 15-17].

Using this approach we have previously shown that the initial stage of pressure infiltration of various alumina and carbon preforms by pure copper obeys universal scaling, as predicted by percolation theory, while latter stages in the process obey the well-known Brooks-Corey relation [16]. These results have been extended to tin-bronze infiltrating packed alumina particle preforms [17], showing that saturation curves shift homothetically as the tin content varies, in agreement with the wetting characteristics of this system. Indeed, according to sessile drop data in the literature [18-21], in Cu-Sn alloys the contact angle θ remains roughly constant while the liquid surface tension σ_{LV} decreases with increasing fraction of tin: if σ_{LV} is doubled with all else constant, then the capillary pressure at given S must double as well.

Here, we vary the contact angle. We infiltrate the same type of alumina preform as in Ref. [17] but now use two alloy systems in which θ depends strongly on alloy composition:

- copper-aluminium, where both θ and σ_{LV} decrease with increasing Al content [21-23] and
- aluminium-tin, where σ_{LV} is roughly constant while θ again decreases markedly at higher Al concentration [24-26].

We explore the relation between these two capillary parameters, θ and σ_{LV}, and the saturation curve. We also compare the work actually spent to effect infiltration with the energy thermodynamically required by the process, this being the work of immersion of the relevant metal/reinforcement system, W_{i}, times the preform specific surface [1, 5-6, 27-29]. W_{i} is related to θ and σ_{LV} via the Young-Dupré equation [18, 30]:

$$W_{\mathrm{i}} \equiv \sigma_{\mathrm{LS}} - \sigma_{\mathrm{SV}} = -\sigma_{\mathrm{LV}} \cos\theta \qquad (2)$$

The final published article is available at Elsevier as: A. Léger, L. Weber and A. Mortensen, "Influence of the wetting angle on capillary forces in pressure infiltration", *Acta Materialia*, Vol. 91 (2015) pp. 57-69 doi:10.1016/j.actamat.2015.03.002.

where σ_{LS} is the solid-liquid interfacial energy and σ_{SV} is the solid surface energy in the initial atmosphere of the infiltration process. Physically, W_i is the energy change that accompanies the replacement of the solid reinforcement free surface with the interface between the solid reinforcement and the liquid metal, per unit area: as such W_i is the thermodynamic driving force or energy barrier (depending on its sign) characteristic of the infiltration process when it is conducted reversibly and without significant change in the total liquid metal surface area [1, 5-6, 27-29].

For the ceramic-metal systems explored here, contact angles are reported to range from strongly non-wetting (128° for Cu) to wetting (64° for Sn-50at.%Al). As will be seen, for all present systems there is no spontaneous infiltration, even with the more wetting alloys. We also show that combining present results plus earlier data for Cu-Sn or pure Hg [17] with relevant sessile drop literature data (which give both σ_{LV} and θ), one obtains a set of master curves that link univocally the measured infiltration pressure for a given saturation, normalized by the relevant σ_{LV} value, with the wetting angle θ. This curve is such that, for the specific alumina preform explored here, over the range $128° \geq \theta \geq 64°$ the saturation curve is proportional, not to W_i, but to a linear function thereof.

Experimental

Materials

Oxygen-free, low phosphorous copper (UNS10300), 99.9% pure tin and aluminium 4N were used, either as pure metal, or after alloying to produce copper-aluminium and tin-aluminium alloys having compositions Cu-50at.%Al, Cu-20at.%Al, Cu-10at.%Al, and Al-10at.%Sn, Al-50at.%Sn or Sn-10at.%Al. Alloying was conducted using a high-vacuum induction furnace under back-filled static argon.

The final published article is available at Elsevier as: A. Léger, L. Weber and A. Mortensen, "Influence of the wetting angle on capillary forces in pressure infiltration", *Acta Materialia*, Vol. 91 (2015) pp. 57-69 doi:10.1016/j.actamat.2015.03.002.

Angular alumina α-Al_2O_3 F1000 particles (similar to those used in Refs [12-13, 15-17]) were purchased from Treibacher Schleifmittel (Laufenburg, Germany); their average diameter is around 5 μm. Porous preforms were prepared by cold isostatic pressing (CIP) of packed cylinders of those powders at 150 MPa during 1 minute. The obtained CIPed preforms were cylindrical, about 14 mm in diameter and 10 mm in height. The alumina volume fraction in the preforms was determined by the ratio of apparent density and reinforcement density, the latter having been determined by He-pycnometry to be $3.876 \cdot 10^3$ kg $\cdot$ m^{-3} [11] (note: the small deviation from the nominal value for alpha-alumina has its origin in the presence of a few internal inclusions of $NaAlO_2$ within the particles). The volume fraction of reinforcing phase in the composites infiltrated and solidified under maximal pressure was either measured by image analysis of optical micrographs using the ImageJ software package (U. S. National Institutes of Health, Bethesda, Maryland, USA) or deduced from Archimedes' principle using a Sartorius MC 210P microbalance of sensitivity ± 10 μg, assuming no residual porosity in the composites. Reproducibility (on the same sample) and variability (across different samples or images) of both procedures are such that the reinforcement volume fraction can be ascertained to ±0.01.

Infiltration experiments

Continuous infiltration

Metal matrix composites were produced by pressure-driven infiltration of ceramic powder preforms with liquid metal. A detailed description of the infiltration apparatus and experimental procedure can be found in Refs [15-16]. In a few words, a CIPed preform is placed beneath a slug of metal inside an alumina crucible in the pressure infiltration apparatus. The metal is heated in vacuum using an induction-heated graphite susceptor situated within the apparatus. After melting, the metal surrounds the preform, and thus seals it from the surrounding atmosphere. Once the infiltration temperature has stabilized to within ± 3 °C, argon gas at stepwise increasing

pressure is let into the infiltration apparatus. This drives the molten metal into the open pores of the preform, infiltrating it from all sides. The volume of metal entering the preform is tracked dynamically by a custom-designed optics-based system measuring the movement of a graphite plunger that floats atop of the liquid metal. At each pressurization step, the pressure is kept constant until metal flow has ceased [13]; the saturation is then recorded and the pressure is increased to the next step. Further details have been given elsewhere [13, 16-17].

At least two separate CIPed angular F1000 preforms were infiltrated with each of either aluminium or tin, and also with each of the six different alloys: Cu-x-at.%Al (x = 50, 20 and 10) at 1100°C, and Sn-x-at.%Al alloys (x = 10, 50, 90) at 1150°C (and at 700°C for pure Sn and Al). The final pressure required for full infiltration (meaning for $S = 1$) was assumed to be reached when the graphite plunger no longer moves detectably after pressure is increased. After complete infiltration, the composite was cooled within the apparatus by switching off the heating while maintaining the applied gas pressure.

Results obtained with the Cu-Al/Al_2O_3 system proved at first to be erratic. After some exploratory experimentation it was found that overheating the sample before infiltration eliminates this problem: the data then become reproducible. Specifically, we found that heating the evacuated preform and the (unpressurized molten) metal under vacuum up to 1300°C and then cooling it down to 1100°C before infiltration at that temperature (instead of heating only to 1100°C and infiltrating), gives reproducible saturation curves when aluminium is present in the alloy. Examination of materials after either of the two heating procedures (straight heating to 1100°C or reaching 1100°C after an excursion to 1300°C) showed no apparent modification of the alumina particles. Infiltration of similar preforms by pure aluminium at 700°C presented the same problem; hence, Al/Al_2O_3 samples were first heated to 1000°C before infiltration at 700°C. The problem was on the other hand not observed at higher temperature: data for infiltration with pure Al after preheating (up to 1300°C followed by infiltration at 1100°C, in the context of Cu-Al

The final published article is available at Elsevier as: A. Léger, L. Weber and A. Mortensen, "Influence of the wetting angle on capillary forces in pressure infiltration", *Acta Materialia*, Vol. 91 (2015) pp. 57-69 doi:10.1016/j.actamat.2015.03.002.

alloy series) were essentially the same as those obtained after heating to 1150°C and infiltrating at that temperature (for the Sn-Al alloy series). The cause for this behaviour is not elucidated; most likely it is caused by interaction between aluminium in the melt and the small partial pressure of oxygen in the atmosphere initially present within the preforms [12].

To sum up, all the experiments involving Cu-Al alloys performed at 1100°C (or also at 700°C for pure Al) were overheated before infiltration, while Sn-Al samples were directly heated and infiltrated at 1150°C or (for pure Sn only) at 700°C.

Partial infiltration

Partial infiltration experiments consisted in infiltrating preforms at a single pressure, which was maintained until the graphite plunger position had stabilized. The partly infiltrated composites were then cooled within the apparatus while maintaining the applied gas pressure. In order to preserve the partly porous sample during metallographic preparation, the metal shell surrounding the preform was first carefully removed (by hand, using steel tooling). Then, remaining open pores of the preforms were evacuated and filled with epoxy through a drilled hole. The samples could then be cut and polished for metallographic examination. The metal/pore relative distribution and its fractal dimension were characterized using thresholded images from two-dimensional metallographic cuts observed in a scanning electron microscope (FEI XLF30, and Zeiss Merlin for pure Al), under backscattered electron mode (to bring out the metal); the procedure is the same as in Refs. [16-17]. The metal fractal dimension was measured by means of the box counting method (using the function "Fractal box counter" of ImageJ; U. S. National Institutes of Health, Bethesda, Maryland, USA). In this method, the fractal dimension D comes from the relation $N(h) \sim h^{-D}$, where $N(h)$ is the number of boxes of linear size h necessary to cover a set of points distributed in a two-dimensional plane. This fractal dimension was measured in the sample central region, where the fraction metal is lowest (nearer to the preform

The final published article is available at Elsevier as: A. Léger, L. Weber and A. Mortensen, "Influence of the wetting angle on capillary forces in pressure infiltration", *Acta Materialia*, Vol. 91 (2015) pp. 57-69 doi:10.1016/j.actamat.2015.03.002.

periphery the metal volume fraction is slightly higher, causing D to increase somewhat as the sampled area approaches the preform periphery [31-33]).

Results

Volume fraction of reinforcement phase

The alumina volume fraction was found to be V_r=0.505±0.015 for all CIPed preforms. On the other hand, the alumina volume fraction determined on the infiltrated samples by either image analysis or densitometry varied from sample to sample, generally spanning the range from 0.50 to 0.61. For the pure aluminium sample infiltrated at 700°C the value measured was smaller than for the empty preform (0.43), while for aluminium infiltrated at 1100°C it was significantly larger (0.56). We further found that the values obtained by densitometry were typically somewhat larger than their image analysis based counterparts.

Saturation curves

Figure 1 compares saturation curves characteristic of the infiltration of CIPed Al_2O_3 preforms by a) Cu-Al alloys (Al, Cu-50at.%Al, Cu-20at.%Al, Cu-10at.%Al and Cu) at 1100°C and b) Sn-Al alloys (Al-10at.%Sn, Sn-50at.%Al, Sn-10at.%Al, Al and Sn) at 1150°C as well as for pure Sn and Al at 700°C, all under stepwise increasing pressure. As seen, adding aluminium to copper lowers significantly the range of pressures required to infiltrate the preform. Saturation curves measured with Sn-Al alloys (Al-10at.%Sn, Sn-50at.%Al, Sn-10at.%Al) are close to one another and are situated at lower pressures than those found with either of the two pure metals, Sn or Al. Increasing the infiltration temperature also lowers the pressure, as can be seen by noting the difference between data collected at 1150°C or at 700°C for both Sn and Al.

The coloured arrows in Fig. 1 represent the final pressure used in partial infiltration experiments with Cu-50at.%Al (1.7 MPa), Cu-10at.%Al (3 MPa), Sn-50at.%Al (0.6 MPa), Sn-10at.%Al (0.9 MPa), Al (1.2 MPa) and Sn (1.3 MPa). SEM micrographs showing the infiltration front for each of these partly infiltrated samples are displayed in Fig. 2. The white square

delineates the area that was used to measure the fractal dimension D_{2D} of the infiltrating metallic front using the box counting method, as in Ref. [16]. The measured fractal dimensions are $D_{2D} = 1.66$ for Cu, 1.64 for Cu-20at.%Sn, 1.62 for Sn, 1.77 for Cu-10at.%Al, 1.72 for Cu-50at.%Al, 1.89 for Sn-10at.%Al and 1.87 for Sn-50at.%Al.

The fractal dimension for the Al/Al_2O_3 composite was not measured because it was difficult to separate the aluminium phase from the alumina particles during the thresholding step (due to weak chemical contrast). As the front is seen to be quite compact, Fig. 2, the fractal dimension D can safely be said to be high for this system too, and close to what was measured with Sn-Al alloys.

Figure 3 shows SEM images (in backscattered electron mode) of fully infiltrated composites with a matrix of Cu, Sn and Cu-50at.%Al (Figs. 3a-b, d obtained with a FEI XLF30 microscope), and with Sn-50at.%Al and Al at 700°C and 1150°C (Figs. 3c, e-f obtained with a Zeiss Merlin microscope). As seen, the composites consist of homogeneously distributed alumina particles in an essentially pore-free metallic matrix. One can however notice that the initially angular particles (clearly visible in the copper and tin matrix, Fig. 3a-b) present a certain degree of blunting (or "rounding") of their sharper angles after infiltration with Cu-Al, Sn-Al alloys and Al at higher temperature (Fig. 3d-f). The effect is less marked at lower temperature when infiltrating with pure Al (see Fig. 3c).

Discussion

Volume fraction of reinforcement phase

Measured V_r values in the as-CIPed preforms vary little, as expected since packing and CIPing procedures were the same for all preforms. The higher V_r values measured using infiltrated composites, and also their greater scatter, suggest that some porosity was present in the final, solidified, composites. Indeed, pores will increase the apparent fraction ceramic when the matrix

is more dense than alumina (as is the case in most present composites), and will increase the fraction alumina in image analysis, given that alumina is the darker phase. This interpretation is further supported by the fact that for aluminium, which is less dense than alumina, densitometry yielded volume fractions that were smaller than 0.505 after infiltration at 700°C, as expected if porosity is present. The most likely source of microporosity in the composites is from solidification shrinkage (no particular measures were taken to assure directional solidification during composite cooldown after infiltration). Note, however, that for the composite infiltrated with aluminium at 1100°C, densitometry yielded higher V_r values (0.56 vs. 0.505); this may signal some degree of alumina densification at higher temperature, this being made possible by the finite rate of alumina diffusion across the melt in this system [34]. We thus use, in all that follows, the volume fraction of the as-CIPed preform as that relevant for interpretation of infiltration experiments, while keeping in mind that there might be an influence of densification or rounding of the alumina particles on the Brooks and Corey parameter λ, as detailed below.

Local wetting: Sessile drop data

Contact angle data for the Cu-Al/Al_2O_3 system at 1150°C from Ref. [21] are displayed in Fig. 4a; in this dataset one notices a transition from non-wetting ($\theta > 90°$) to wetting ($\theta < 90°$) as the Al content increases. More recently, Schmitz *et al.* also measured the contact angle θ for this system [22] using the dispensed drop technique at 1100°C for liquid Al, Cu and their alloys on sapphire surfaces with three different crystallographic orientations, namely ((0001), $(11\bar{2}0)$ and $(1\bar{1}02)$). These authors reported the highest contact angles for the (0001) orientation. Now, in our samples, with aluminium present in the melt, there is some degree of liquid/solid interface migration by dissolution-reprecipitation, Fig. 3; see also Ref. [34]. Therefore, it is likely that the shape of the particles evolve towards orientations of low σ_{SL}. In quoting the data of Schmitz *et al.*, we have therefore opted to use their lower measured contact angle values, by taking the

average between values of the orientation $(11\bar{2}0)$ and $(1\bar{1}02)$ as an average value characteristic of the particle surface. Schmitz *et al.* also found that the Cu-Al alloy contact angle varies during roughly one minute before it stabilizes at a fixed value. Since significantly more than a minute was allowed for stabilization of the saturation after each pressure increment, we use here their final, stabilized, contact angle values in data interpretation; these are plotted in Fig. 4a. The surface tension σ_{LV} for the Cu-Al system was measured using electromagnetic levitation in Ref [23]; we use here those data for σ_{LV}, Fig. 4b.

The evolution of the contact angle θ at 1100°C for Sn-Al/Al_2O_3 versus the at.%Al is displayed in Fig. 4c, from measurements in Ref. [25]. Here too, θ falls below 90°. It decreases both when aluminium is added to tin or when tin is added to aluminium, and reaches its minimum value between 15 and 30 at.%Al [25]. Data for the surface tension in that system at temperatures from 700 to 1000°C can be found in Ref. [26]: the addition of tin to aluminium gives rise to an abrupt reduction in surface tension, which is already closer to that of Sn than that of Al with only 4 at.% Sn in Al. To estimate values of Sn-Al alloy surface tensions in infiltration experiments of this work, we have extrapolated to 1150°C lines traced through lower temperature data by authors of Ref. [26] in Fig. 5 of that reference. The curve in Fig. 4d was then traced by ourselves through those extrapolated data points, taking a value of 497 mJ/m^2 for the surface tension of pure tin following Eq. 14 of Ref. [35], and a value of 798 mJ/m^2 for pure aluminium (which is an average value of the two linear regressions from Fig. 17 of Ref [36]) at 1150 °C.

Global wetting: Saturation curves

Saturation curves for both systems, Cu-Al/Al_2O_3 at 1100°C and Sn-Al/Al_2O_3 at 1150°C, Fig. 1, have the usual shape: infiltration starts at a specific threshold pressure P_c, progresses rapidly as P increases, then gradually approaches full saturation ($S = 1$) in asymptotic fashion. In earlier

The final published article is available at Elsevier as: A. Léger, L. Weber and A. Mortensen, "Influence of the wetting angle on capillary forces in pressure infiltration", *Acta Materialia*, Vol. 91 (2015) pp. 57-69 doi:10.1016/j.actamat.2015.03.002.

work, the infiltration of similar alumina preforms by pure copper [16] and by copper-tin alloys [17], was shown to be governed by percolation in its initial stages.

At low saturation, infiltration is indeed known to be an embodiment of a variant of percolation known as invasion percolation: to be infiltrated with metal, a pore must be sufficiently large but it must also be connected to a stringer of other sufficiently large pores that stretches to regions where the metal is injected into the preform (the preform periphery in the present experiments). Percolation theory predicts that, just past the percolation threshold, the cluster of invaded pores is a fractal of dimension $D_{3D} = 2.52$ [37-40]. If a few simple and reasonable assumptions are made concerning pore geometry, it can also be shown that, in this initial phase of the infiltration process, the saturation curve should follow the following universal scaling law [16, 41]:

$$S = C(P - P_c)^{\beta} \tag{3}$$

where P_c is a threshold pressure, C is a system-dependent constant and $\beta = 0.41$, whatever the 3D pore structure (hence the "universality" of this scaling law).

When plotting the saturation curves of Fig. 1 in coordinates of $S^{(1/0.41)}$ versus P to test Eq. (3), one finds that data conform indeed with Eq. (3) in initial phases of infiltration, and do so up to a saturation near $S = 0.7$, Fig. 5 (left). Data presented here thus extend, to lower wetting angles, what was documented in Refs. [16-17] for Cu and Cu-Sn alloys, namely that initial phases of the pore invasion process are governed by percolation.

Figure 6 replots the initial (low saturation) data of all saturation curves of this work, together with similar curves from Ref. [17] for Cu-Sn alloys infiltrating the same preforms, after division of the applied pressure P by the measured threshold (critical percolation) pressure P_c for each metal or alloy. As seen, for all non-wetting alloys ($\theta \geq 90°$; blue, red and orange points) this collapses almost all the curves into a narrow band. In other words, in the regime of percolation-dominated infiltration, the scaling law given in Eq. (3) can be rewritten as:

The final published article is available at Elsevier as: A. Léger, L. Weber and A. Mortensen, "Influence of the wetting angle on capillary forces in pressure infiltration", *Acta Materialia*, Vol. 91 (2015) pp. 57-69 doi:10.1016/j.actamat.2015.03.002.

$$S = K\left(\frac{P}{P_c} - 1\right)^{\beta} \tag{4}$$

where K depends on the solid porous material that is infiltrated but varies only weakly with wetting characteristics of the fluid. For the present type of packed alumina ceramic particle preform K is situated between 1.2 and 1.7, increases slowly as θ decreases, then drops to ≈0.8 for systems having a contact angle less than 65°, Fig. 6. This observation remains to be confirmed for other preforms or wider ranges of variation of the wetting angle; however, it represents an interesting reduction in the number of parameters that enter the law describing the initial, percolation-dominated, flow path of the matrix into the preform for systems such that $\theta \geq 90°$. Note also how the universal scaling law given in Eqs. 3 and 4 remains valid with systems where $\theta < 90°$ (although the parameter K is not constant) despite the fact that a reduction in the contact angle causes an increase in the fractal dimension of the liquid infiltrant cluster, and hence in the infiltrating liquid flow path, during initial phases of infiltration, Fig. 2.

At higher saturation universality is lost and the saturation curves follow a semi-empirical law known as the Brooks-Corey correlation [8, 43-44], Fig. 5, right-hand curves. The Brooks-Corey correlation, which has amply been documented to govern saturation curves characteristic of many fluid/solid systems including metal/ceramic composites [10, 12-17, 45-48], links the saturation S and the capillary pressure P with the power-law:

$$S = 1 - \left(\frac{P_b}{P}\right)^{\lambda} \qquad \text{for} \qquad P \geq P_b \tag{5}$$

where P_b is called the "bubbling pressure" (a constant characteristic of both the fluid and the solid, which comes close, but is generally not equal, to P_c), and λ is a "pore size distribution index" related to the shape and size distribution of open pores in the infiltrated porous solid. As seen in Fig. 5, as in previous experiments with pure Cu and Cu-Sn alloys, here too the Brooks-Corey correlation is obeyed at higher saturation, although the level of agreement is somewhat lower with the more highly wetting alloys. Present data also confirm another conclusion of Refs.

[16-17], namely that the cross-over from a dominance of throat size distribution statistics in the early phases of infiltration (meaning a governance of infiltration by the physics of invasion percolation) to a dominance of the average pore size and shape in later phases of the infiltration process (where the Brooks-Corey correlation is obeyed) is very gradual, both laws being obeyed over a relatively wide range of saturation, Fig. 5.

An interesting finding that emerges from the present data is that the pore size distribution index λ (which we computed by passing a straight line in right-hand plots of Fig. 5 through data in the range $-1 > \ln(1-S) > -2.2$, corresponding to $0.6 \leq S \leq 0.9$), does not only depend on the pore geometry: it increases gradually with the Al content (from 4.1 for Cu to 5 for Cu-50at.%Al). The value of λ is higher for aluminium bronze than it was for similar preforms infiltrated by pure copper or tin bronze ($\lambda = 3.7 \pm 0.4$) [17] (we note in passing that in the case of pure aluminium, the graphite plunger movement never clearly stabilized at constant pressure, meaning that λ is probably more than the value we report here for this system: $\lambda > 7$). For the Sn-Al system, it was difficult to measure a clear value for the Brooks-Corey exponent λ; still, data suggest that λ for Sn-10at.%Al is slightly higher than for Cu or Cu-Sn alloys, being in the range between 4 and 5. For Al-10at.%Sn λ is again high, and lies near the value found with pure Al, Fig. 5b, right-hand plot.

Two reasons can be given to explain why λ increases with increasing amount of aluminium in copper or tin. The first is simply the fact that, as one adds aluminium to copper and, *a fortiori*, with Sn-Al alloys, θ falls below 90° (the value below which the melt will for example spontaneously infiltrate a straight cylindrical pore). It is known from percolation simulations that, in the later stages of infiltration, where the Brooks-Corey correlation describes infiltration pressures, every remaining uninfiltrated pore should be accessible to metal (*i.e.,* should have at least one metal-filled neighbouring pore) [17, 33, 49-50]. The range of pressures required to

complete the infiltration process should therefore depend primarily on local pore geometrical characteristics, and of course on pore size. Now, the flow path of the metal into, and then within, each pore must depend on θ. Consideration of the narrowest, converging, crevices in the preforms exemplifies this: these are the last preform regions to be infiltrated when θ exceeds 90°, but are spontaneously filled with metal whenever it enters the pore if $\theta < 90°$. With $\theta > 90°$ these crevices will govern the last, high-*P*, portion of the saturation curve, while these same crevices simply become part of the volume that is *first* infiltrated whenever metal penetrates a pore if $\theta <$ 90°, such that their influence will appear on the mid-range of *S* or *P* values along the saturation curve. Hence, λ should increase as θ decreases below 90°: this is indeed the trend that is observed here, Fig. 5.

A second reason why λ might vary resides in the fact that aluminium additions to tin or copper also cause alumina dissolution/reprecipitation within the melt. This is visible in fully infiltrated composites (Fig. 3d-f) and was already reported for similar Al_2O_3 particles infiltrated by Cu-Al alloys at 1200 °C in Ref. [34]. Essentially the same effect is documented in the sessile drop literature in the form of triple line ridging [51-54] and dissolution of sapphire substrates [55-57] at comparable temperature and time scales. Here, as in sessile drop experiments, solid phase transport through the liquid may open or close flow paths for the molten metal as it invades preform pores and may enable densification of the preform. Such effects are suggested by densitometry measurements for composites infiltrated with pure aluminium at 1100°C, and can also affect the Brooks and Corey exponent λ. These two factors do not always vary in the same direction (for example, pure Al shows significantly different wetting angles between 1100-1150 °C and 700 °C yet, although less pronounced at 700°C, there is at both temperatures solution/reprecipitation of alumina in aluminium, Fig. 3c); however, we do not believe that the present data suffice to conclude whether one or the other effect exerts a dominant influence.

The final published article is available at Elsevier as: A. Léger, L. Weber and A. Mortensen, "Influence of the wetting angle on capillary forces in pressure infiltration", *Acta Materialia*, Vol. 91 (2015) pp. 57-69 doi:10.1016/j.actamat.2015.03.002.

Metal fractal dimension

SEM images of partly infiltrated fronts for these alloys, Fig. 2, show a differentiation (clearly pronounced with Sn-Al alloys or pure Al) from the highly branched, fractal percolation-dominated invasion front that is observed with Cu, Sn and their alloys (Figs. 2 a-c; see also Refs [16-17]) to an increasingly compact front as one moves to Cu-Al alloys (Figs. 2 d & e), then to Sn-Al alloys (Figs. 2 f & g), and finally to pure Al (Fig. 2h).

This observation is consistent with measured values of D at the infiltration front for these various systems. D (in two dimensions) is between 1.6 and 1.7 for similar CIPed F1000 Al_2O_3 preforms infiltrated by Cu, Sn and their alloys, as predicted by percolation theory, Figs. 2 a-c and Refs [16-17]. For Cu-Al alloys, the measured D value is somewhat higher (1.77 for Cu-10at.%Al and 1.72 for Cu-50at.%Al). For Al-Sn alloys, the front becomes visibly more compact, and indeed the measured metal phase fractal dimensions come close to $D = 2$, the value expected for a non-fractal object (1.89 for Sn-10at.%Al and 1.87 for Sn-50at.%Al). This observed trend of increasing D with decreasing θ is in line with earlier work in literature [33,37-39, 58-62]. Note, however, that there is no concomitant deviation from the (universal) saturation law that governs the initial, percolation-dominated, stage of infiltration (Fig. 6).

Dependence of infiltration pressure on the contact angle and on the work of immersion

In work to date on infiltration by non-wetting metals, the saturation curve has by and large had a shape determined only by the pore geometry: changing the alloy composition, and hence its local wetting characteristics, resulted in a homothetical shift of the saturation curve along the pressure axis, this shift being proportional to the work of immersion W_i [11-13, 15, 48, 63-65]. This can be rationalized by equating the work of immersion W_i, *i.e.,* the work required to exchange the solid vapour interface by a solid liquid interface times the specific surface of the

preform, to the total work W exerted on the liquid, or in other words by assuming that irreversible energy losses, e.g. by viscosity or Haines jumps [7-8, 49, 66] are comparatively small:

$$W = (1 - V_r) \int_0^1 P \, dS = \Delta E_r \equiv A_S \, V_r \, \rho_{alumina} \, W_i \qquad (6)$$

where $\Delta E_r \equiv A_S \, V_r \, \rho_{alumina} \, W_i$ is the reversible work of infiltration for the system at hand, A_S is the specific surface of the alumina particles (A_S = 1160 ± 56 m^2/kg for the present preforms [17]) and $\rho_{alumina}$ is the density of this alumina (3.876 · 10^3 kg · m^{-3} [11]). If, additionally, the infiltration path of the metal remains the same as W_i changes, then one is also entitled to expect that, as W_i changes, saturation curves will simply move homothetically along the horizontal, with the infiltration pressure at each saturation S remaining proportional to W_i.

If one extends this analysis to θ values near and below 90°, one then expects that W will decrease and then vanish (at θ = 90°) before becoming negative. This is not what we observe here: while the pressure-saturation integral decreases with decreasing θ it remains positive at least down to θ=64° (characteristic for the Al-50at.%Sn alloy). Infiltration with a wetting fluid thus requires a finite pressure. This is in keeping with data in the literature for non-metallic liquids: these show that spontaneous infiltration is only observed when θ is near zero, and that there is an "intermediate wetting" regime, in which flow of the liquid in either direction, into or out of a porous body, requires that pressure be applied to drive motion in the desired direction [49, 67-73]. The same has also been observed for metal/ceramic systems: Narciso *et al.* infiltrated packed Al_2O_3 particulates by pure silver (containing dissolved oxygen) for which θ < 90° and nevertheless measured a positive threshold pressure that must be overcome to drive infiltration [74]. Travitzky and Shlayen found, for Cu-O melts infiltrated into α-Al_2O_3, that the threshold for spontaneous infiltration was for θ between 32° and 44° [68].

The final published article is available at Elsevier as: A. Léger, L. Weber and A. Mortensen, "Influence of the wetting angle on capillary forces in pressure infiltration", *Acta Materialia*, Vol. 91 (2015) pp. 57-69 doi:10.1016/j.actamat.2015.03.002.

Table 1 lists for each infiltration experiment the apparent work of infiltration, $W_{i,app}$, obtained by integrating the saturation curve with respect to saturation and dividing this integral by the total preform/infiltrant interface area created per unit volume of preform (see Eq. 6):

$$W_{i,app} = \frac{(1-V_r)\int_0^1 P\, dS}{A_S\, V_r\, \rho_{alumina}} \qquad (7)$$

Table 1 also gives corresponding values of W_i according to sessile drop data (Eq. 2) for Cu-Al/Al_2O_3 and Sn-Al/Al_2O_3, computed using values of σ_{LV} and θ from Fig. 4, and includes data in Ref. [17] for Cu-Sn alloys infiltrating similar Al_2O_3 particle preforms. Taking the ratio of $W_{i,app}$ to W_i, Table 1, one finds that: (i) this ratio remains close to or only slightly higher than unity (by up to roughly 40%) for clearly non-wetting systems (all metals and alloys across the Cu-Sn system plus Hg, for which $\theta > 120°$), and then (ii) increases to far higher values (1.6 to 5) before (iii) becoming negative as θ falls below 110° and 90°, respectively.

If we plot $W_{i,app}$ normalized by σ_{LV} as a function of $\cos\theta$, the data congregate along a straight line that passes through the point ($\cos\theta = 1$; $\frac{W_{i,app}}{\sigma_{LV}} = 0$) with a slope of -0.47, cf. Fig. 7, implying for the θ range investigated here that:

$$W_{i,app} = -0.47\sigma_{LV}(\cos\theta - 1) = 0.47(W_i + \sigma_{LV}). \qquad (8)$$

Data points for the highest wetting angles (high negative $\cos\theta$) seem on the other hand roughly aligned along the line passing through the origin and of slope (-1); this is as expected if $W_{i,app} = W_i$.

Figure 8 plots the infiltration pressures P corresponding to specific values of the saturation S (0^+, 0.3, 0.5, 0.95) normalised by σ_{LV} versus $\cos\theta$, together with similar data obtained for Cu in Ref. [16] and Cu-Sn in Ref. [17]. The threshold pressure P_c in Fig. 8a was determined for all experiments by linear regression of data plotted as $S^{(1/0.41)}$ vs. P over the range $0.02 \leq S^{(1/0.41)} \leq 0.35$ (corresponding to $0.2 \leq S \leq 0.65$). The pressure corresponding to a saturation of 0.95 was deduced from the linear regression obtained in the range of $-1 > \ln(1-S) > -2.2$ (corresponding to roughly $0.6 \leq S \leq 0.9$) in the (Brooks and Corey) coordinates that are used in the right-hand

plots of Fig. 5. As seen, for the three lower saturations ($S = 0^+$, 0.2, 0.5), the pressure P that is required for infiltration can again roughly be fitted by a straight line going through the origin. This can be written (using Eq. 2):

$$P \propto \sigma_{\mathrm{LV}}(1-\cos\theta) = \sigma_{\mathrm{LV}} - \sigma_{\mathrm{LV}}\cos\theta = W_{\mathrm{i}} + \sigma_{\mathrm{LV}} \qquad (9)$$

for all three saturations (less so for $S = 0.95$, as the line through data does not go through the point of coordinates (1, 0) on the plot).

Taken at face value, Eqs. 8 and 9 would suggest that infiltration, at each saturation and in total, corresponds to the creation of a certain area of metal/ceramic interface plus a roughly equal area of liquid metal meniscuses. This, however, cannot hold, at the very least in the last phases of infiltration, since the proportion of liquid/solid interfaces then far exceeds that of liquid/vapour interfaces (a similar conclusion was reached, using quantitative metallography in soil infiltrated with non-metallic liquid, by Morrow [7]). An elucidation of these effects will require (i) detailed numerical simulations of infiltration in both low (percolation-dominated) and high (local pore geometry dominated) phases of infiltration that take into account the complex nature of the pore space present in packed particle preforms such as those in this work and also the complex metal flow path, (ii) experiments similar to those of this work but with several other preforms, to probe whether expressions in Eqs. (8) and (9) remain valid (these are underway), and (iii) an exploration of more strongly non-wetting systems. These last experiments would be interesting since, in principle, the straight line that can be drawn through data in Fig. 7, and probably also in Fig. 8d, must bend upwards, since full preform infiltration cannot require *less* energy than is dictated by thermodynamics in Eq. 6. As already mentioned, the data in Fig. 7 actually show hints of this.

Finally, a comparison can be attempted between the threshold pressure for infiltration of the particle preforms, P_c, and geometrical estimates of the pressure required to push a smooth, macroscopically planar, front of metal through periodically packed sphere assemblies [72, 76-79]. Figure 9 compares the present experimental data for P_c normalized by the metal or alloy surface

tension and multiplied by the average particle radius of alumina particles in preforms of this work (r = 2.5 μm) with predictions for both square and hexagonal close-packed spheres given by the model of Mason and Morrow [80] and by the numerical data of Slobozhanin *et al.* [81] obtained using the Surface Evolver software [82]. The numerical results of Hilden and Trumble [83] using the same software for the special configuration of hexagonal packed sphere separated by 1/10 their radius are also plotted in Fig. 9. One finds that:

(i) the various packed sphere predictions differ considerably, both quantitatively and qualitatively from one another (peak capillary pressures for $0 < \theta < 90°$ differ by a factor of 2.5), and

(ii) that our data for P_c are situated between the different hexagonal close-packed configurations (close and separated by 0.1*radius) for high θ, while measured values lie above predictions of all models when $\theta < 90°$. Furthermore, the slope of the line through data for P_c is lower than for any of these packed sphere models. Thus, although such predictions capture the right order of magnitude for P_c, they fail to predict its dependence on θ. This is not surprising since (i) the present particles are neither spherical nor packed in a regular arrangement (while one sees by mutual comparison of numerical results that the precise sphere arrangement matters) and (ii) most importantly since, as shown earlier [16], metal penetration into packed particle preforms is first dominated by the statistics and connectivity of throats separating irregular pores, and as such differs fundamentally from what was assumed in simulations of the directional infiltration of variously packed monosized spheres.

Conclusions

From experiments presented in this work, the following conclusions can be drawn:

The final published article is available at Elsevier as: A. Léger, L. Weber and A. Mortensen, "Influence of the wetting angle on capillary forces in pressure infiltration", *Acta Materialia*, Vol. 91 (2015) pp. 57-69 doi:10.1016/j.actamat.2015.03.002.

• Entire saturation curves characterizing capillarity in high-temperature infiltration of porous Al_2O_3 particle preforms by Cu-Al and Al-Sn alloys across the binary alloy composition range at 1100°C-1150°C can be obtained with high precision in one single infiltration run for each alloy composition and temperature; however, overheating Cu-Al alloy (to 1300°C) before infiltration was found to be necessary to obtain reproducible curves.

• Adding aluminium to pure copper or tin maintains the two regimes of infiltration that were shown in earlier work to govern the saturation curves, namely (i) the early percolation-dominated phases and (ii) the later, pore geometry dominated regime, described by the Brooks and Corey correlation.

• In the first, percolation-dominated, phase all measured saturation curves collapse into one single curve if the pressure is normalized by the threshold percolation pressure P_c; at low saturations this curve has the universal scaling form dictated by percolation theory.

• With increasing Al content in either Cu or Sn there is (i) at low saturation an increase of the compactness and in the fractal dimension D_{3D} of the infiltrated metal cluster and (ii) at higher saturations an increase in the pore size distribution index λ of the Brooks and Corey correlation.

• The pressure P required to reach a fixed saturation (0^+, 0.3, 0.5), normalized by the corresponding metal or alloy surface tension and plotted as a function of $\cos\theta$, can roughly be fitted with a straight line that passes through the point of coordinates ($\cos\theta = 1$, 0). The line does not pass through the origin as would be the case were these pressures proportional to the work of immersion.

• A similar correlation is found for the total work required to effect full infiltration. Data points for the more poorly wetting systems explored show, furthermore, that the total energy required for full infiltration roughly equals the reversible work of infiltration theoretically required on the basis of thermodynamic data for the systems at hand. For lower values of θ, on the other hand, irreversible energy losses become dominant.

The final published article is available at Elsevier as: A. Léger, L. Weber and A. Mortensen, "Influence of the wetting angle on capillary forces in pressure infiltration", *Acta Materialia*, Vol. 91 (2015) pp. 57-69 doi:10.1016/j.actamat.2015.03.002.

• Simple packed sphere models capture the order of magnitude, but neither the precise value nor the dependence on θ, of the threshold pressure required to initiate infiltration of packed particle beds.

Acknowledgements

This work was sponsored by the Swiss National Science Foundation, Project No. 200020-137685. We gratefully acknowledge Willy Dufour, Raphael Charvet, Claudio Bacciarini, Cyril Dénéréaz and Dr. Noelia Calderon for their assistance in the design and construction of the infiltration apparatus used here, Dr. José-Miguel Molina-Jorda of the University of Alicante and Prof. W.C. Carter, of the Massachusetts Institute of Technology, for many stimulating discussions on both the present results, the general scientific context of this work, and its ramifications.

The final published article is available at Elsevier as: A. Léger, L. Weber and A. Mortensen, "Influence of the wetting angle on capillary forces in pressure infiltration", *Acta Materialia*, Vol. 91 (2015) pp. 57-69 doi:10.1016/j.actamat.2015.03.002.

References

[1] Mortensen A. Melt infiltration of metal matrix composite. In: Clyne TW, editor. Comprehensive composite materials, vol. 3. Oxford: Pergamon, 2000. p.521.

[2] Chawla N, Chawla KK. Metal matrix composites. New York: Springer Verlag, 2006.

[3] Asthana R. Solidification processing of reinforced metals. Uetikon-Zurich: Trans-Tech Publications, 1998.

[4] Evans A, SanMarchi C, Mortensen A. Metal matrix composites in industry: an introduction and a survey. Dordrecht NL: Kluwer Academic Publishers, 2003.

[5] Mortensen A, Jin I. Int Mater Rev 1992;37:101.

[6] Michaud V, Mortensen A. Compos part A-Appl S 2001;32:981.

[7] Morrow NR. Ind Eng Chem 1970;62:32.

[8] Bear J. Dynamics of fluids in porous media. New York: American Elsevier, 1972.

[9] Kaufmann H, Mortensen A. Metall and Mat Trans A 1992;23:2071.

[10] Michaud VJ, Compton L, Mortensen A. Metall Trans A 1994;25:2145.

[11] Bahraini M. Characterization of capillary forces during liquid metal infiltration, EPFL doctoral thesis 3787. Ecole Polytechnique Fédérale de Lausanne, 2007.

[12] Bahraini M, Weber L, Narciso J, Mortensen A. J Mater Sci 2005;40:2487.

[13] Léger A, Calderon NR, Charvet R, Dufour W, Bacciarini C, Weber L, Mortensen A. J Mater Sci 2012;47:8419

[14] Molina J, Bahraini M, Weber L, Mortensen A. J Mater Sci 2008;43:5061.

[15] Bahraini M, Molina JM, Kida M, Weber L, Narciso J, Mortensen A. Curr Opin Solid State Mater Sci 2005;9:196.

[16] Léger A, Weber L, Mortensen A. Mater Res Lett 2014; in print, available on-line (DOI:10.1080/21663831.2014.948692)

[17] Léger A, Molina JM, Weber L, Mortensen A. J Mater Sci 2014;49;7669.

[18] Eustathopoulos N, Nicholas MG, Drevet B. Wettability at high temperature. Amsterdam: Pergamon-Elsevier Science, 1999.

[19] Lee J, Shimoda W, Tanaka T. Mater Trans 2004;45:2864.

[20] Ricci E, Giuranno D, Grosso I, Lanata T, Amore S, Novakovic R, Arato E. J Chem Eng Data 2009;54:1660.

[21] Li JG, Coudurier L, Eustathopoulos N. J Mater Sci 1989;24:1109.

[22] Schmitz J, Egry I, Brillo J. J Mater Sci 2014;49:2286.

[23] Schmitz J, Brillo J, Egry I, Schmid-Fetzer R. Inter J Mater Res 2009;100:1529.

[24] Goumiri L, Joud JC, Desre P. Surf Sci 1979;88:461.

[25] Li JG, Chatain D, Coudurier L, Eustathopoulos N. J Mater Sci Lett 1988;7:961.

[26] Goumiri L, Joud JC, Desre P, Hicter JM. Surf Sci 1979;83:471.

[27] Mortensen A, Cornie JA. Metall Trans A 1987;18:1160.

[28] Michaud V, Mortensen A. Scripta Mater 2007;56:859.

[29] Michaud V, Mortensen A. Scripta Mater 2012;67:519.

[30] Eustathopoulos N, Mortensen A. Capillary phenomena, interfacial bonding and reactivity. In: Suresh S, Mortensen A, Needleman A, editors. Fundamentals of metal matrix composites Stoneham, Mass: Butterworth-Heinemann, 1993.

[31] Lenormand R Proc Roy Soc London 1989;A423:159.

[32] Hunt A, Ewing R. Percolation theory for flow in porous media. Heidelberg: Springer, 2009.

[33] Sahimi M. Flow and Transport in Porous Media and Fractured Rock: From Classical Methods to Modern Approaches, 2nd Edition. Germany: Wiley-VCH Verlag, 2011.

[34] Krüger C, Mortensen A. J Mater Sci 2012;47:6346.

[35] Novakovic R, Giuranno D, Ricci E, Lanata T. Surf Sci 2008;602:1957.

[36] Keene BJ. Inter Mater Rev 1993;38:157.

[37] Wilkinson D. Phys Rev A 1986;34:1380.

[38] Stauffer D, Aharony A. Introduction to percolation theory - revised second edition. Boca Raton USA: CRC Press, 1994.

[39] Gouyet JF. Physics and fractal structures: Masson, Paris and Springer, New York, 1996.

[40] Sahimi M. Applications or Percolation Theory: Taylor and Francis, London UK, 1994.

[41] Clément E, Baudet C, Guyon E, Hulin JP. J Phys D Appl Phys 1987;20.

[42] Higbie J. Am J Phys 1991;59:184.

[43] Dullien FAL. Porous media, fluid transport and pore structure. New York: Academic Press, 1979.

[44] Brooks RH, Corey AT. Hydraulic Properties of Porous Media. 3: Colorado State University Hydrology Papers, 1964. p.27.

[45] Dopler T, Modaressi A, Michaud VJ. Metall Mater Trans B 2000;31:225.

[46] Rodriguez A, Sanchez S, Narciso J, Louis E, Rodriguez-Reinoso F. J Mater Sci 2005;40:2519.

[47] Molina JM, Arpon R, Saravanan RA, GarciaCordovilla C, Louis E, Narciso J. Scripta Mater 2004;51:623.

[48] Kida M, Bahraini M, Molina JM, Weber L, Mortensen A. Mater Sci Eng A 2008;495:197.

[49] Dullien FAL. Porous Media, Fluid Transport and Pore Structure - Second Edition. New York: Academic Press Inc., Harcourt Brace Jovanovich Publishers, San Diego, USA, 1992.

[50] Chatzis I, Dullien FAL. J Can petrol technol 1977;16:97.

[51] Saiz E, Tomsia AP, Cannon RM. Acta Mater 1998;46:2349.

[52] Saiz E, Cannon RM, Tomsia AP. Acta Mater 1999;47:4209.

[53] Saiz E, Cannon RM, Tomsia AP. Acta Mater 2000;48:4449.

[54] Saiz E, Tomsia AP, Suganuma K. J Eur Ceram Soc 2003;23:2787.

The final published article is available at Elsevier as: A. Léger, L. Weber and A. Mortensen, "Influence of the wetting angle on capillary forces in pressure infiltration", *Acta Materialia*, Vol. 91 (2015) pp. 57-69 doi:10.1016/j.actamat.2015.03.002.

[55] Laurent V, Chatain D, Chatillon C, Eustathopoulos N. Acta Metall 1988;36:1797.

[56] Zhou XB, De Hosson JTM. J Mater Sci 1995;30:3571.

[57] Levi G, Kaplan WD. Acta Mater 2002;50:75.

[58] Lenormand R. Physica A 1986;140:114.

[59] Lenormand R. Journal of Physics: Condensed Matter 1990;2:SA79.

[60] Cieplak M, Robbins MO. Phys Rev Lett 1988;60:2042.

[61] Cieplak M, Robbins MO. Phys Rev B 1990;41:11508.

[62] Martys N, Robbins MO, Cieplak M. Physical Review B 1991;44:12294.

[63] Molina JM, Rodriguez-Guerrero A, Bahraini M, Weber L, Narciso J, Rodriguez-Reinoso F, Louis E, Mortensen A. Scripta Mater 2007;56:991.

[64] Bahraini M, Molina JM, Weber L, Mortensen A. Mater Sci Eng A 2008;495:203.

[65] Mortensen A, Wong T. Metall Trans A 1990;21A:2257.

[66] Mortensen A. Mater Sci Eng A 1991;135:1.

[67] Gonzalez EJ, Trumble KP. J Amer Ceram Soc 1996;79:114.

[68] Travitzky NA, Shlayen A. Mater Sci Eng A 1998;244:154.

[69] Kennedy AR, Wood JD, Weager BM. J Mater Sci 2000;35:2909.

[70] Yang YW, Zografi G, Miller EE. J Colloid Interf Sci 1988;122:24.

[71] Yang YW, Zografi G, Miller EE. J Colloid Interf Sci 1988;122:35.

[72] Bán S, Wolfram E, Rohrsetzer S. Colloid Surface 1987;22:291.

[73] Anderson WG. Journal of Petroleum Technology 1987;39:1283.

[74] Narciso J, Garcia-Cordovilla C, Louis E. Scripta Mater 1997;36:363.

[75] León y León CA. Adv Colloid Interf 1998;76–77:341.

[76] Trumble KP. Acta Mater 1998;46:2363.

[77] Yang XF, Xi XM. J Mater Sci 1995;30:5099.

The final published article is available at Elsevier as: A. Léger, L. Weber and A. Mortensen, "Influence of the wetting angle on capillary forces in pressure infiltration", *Acta Materialia*, Vol. 91 (2015) pp. 57-69 doi:10.1016/j.actamat.2015.03.002.

[78] Frage N, Froumin N, Rubinovich L, Dariel MP. 15 International Plansee seminar, Plansee Holding 2001.

[79] Hamlett CAE, Shirtcliffe NJ, McHale G, Ahn S, Bryant R, Doerr SH, Newton MI. Environ Sci Technol 2011;45:9666.

[80] Mason G, Morrow NR. J Colloid Interf Sci 1994;168:130.

[81] Slobozhanin LA, Alexander JID, Collicott SH, Gonzalez SR. Phys Fluids 2006;18.

[82] Brakke K. Experiment Math vol 1, 1992;1:141.

[83] Hilden JL, Trumble KP. J Colloid Interf Sci 2003;267:463.

The final published article is available at Elsevier as: A. Léger, L. Weber and A. Mortensen, "Influence of the wetting angle on capillary forces in pressure infiltration", *Acta Materialia*, Vol. 91 (2015) pp. 57-69 doi:10.1016/j.actamat.2015.03.002.

LIST OF TABLES

Table 1 - Work $W_{i,app}$ computed by integration of saturation curve divided by total preform/infiltrant interface area created per unit volume of preform (Eq. 7) and W_i computed using sessile drop data (Eq. 2) for Cu-Al/Al_2O_3 at 1100°C and Sn-Al/Al_2O_3 at 1150°C. Values for θ and σ_{LV} are from Fig. 4. For Hg, we have taken σ_{LV} = 486 mJ/m^2 [36] and two different values of θ (127° and 142°) according to Ref [75] and for infiltration at 700°C, for Al: σ_{LV} = 874 mJ/m^2 [36] and θ= 100° [55] and for Sn : σ_{LV} = 526 mJ/m^2 [35] and θ = 140° [18].

Metal/Al_2O_3	$W_{i,app}$ (Eq.7) (mJ/m^2)	θ	W_i (Eq.2) (mJ/m^2)	$W_{i,app}/W_i$	θ	W_i (Eq.2) (mJ/m^2)	$W_{i,app}/W_i$
		from [18]					
Sn (700°C)	440	140	403	**1.09**			
		from [75]			from [75]		
Hg (T_{room})	423	142	383	**1.10**	127	292	**1.45**
		from [55]					
Al (700°C)	463	100	152	**3.05**			
		from [21]			from [22]		
Cu (1100-1150°C)	934	128	825	**1.13**	116	573	**1.63**
Cu-5at.%Sn (1150°C)	855	128	708	**1.21**			
Cu-10at.%Sn (1150°C)	767	128	616	**1.25**			
Cu-20at.%Sn (1150°C)	500	126	458	**1.09**			
Cu-40at.%Sn (1150°C)	407	122	318	**1.28**			
Cu-50at.%Sn (1150°C)	367	122	297	**1.24**			
Sn (1150°C)	359	122	263	**1.37**			
Cu-10at.%Al (1100°C)	776	115	566	**1.37**	110	458	**1.69**
Cu-20at.%Al (1100°C)	622	102	264	**2.36**	105	329	**1.89**
Cu-50at.%Al (1100°C)	444	80	-177	**-2.51**	95	89	**4.99**
Sn-10%at.%Al (1150°C)	194	89	-9	**-21.56**			
Al (1100-1150°C)	262	71	-260	**-1.01**	86	-56	**-4.68**
Al-10%at.%Sn (1150°C)	154	69	-202	**-0.76**			
Sn-50%at.%Al (1150°C)	150	64	-231	**-0.65**			

The final published article is available at Elsevier as: A. Léger, L. Weber and A. Mortensen, "Influence of the wetting angle on capillary forces in pressure infiltration", *Acta Materialia*, Vol. 91 (2015) pp. 57-69 doi:10.1016/j.actamat.2015.03.002.

LIST OF FIGURES

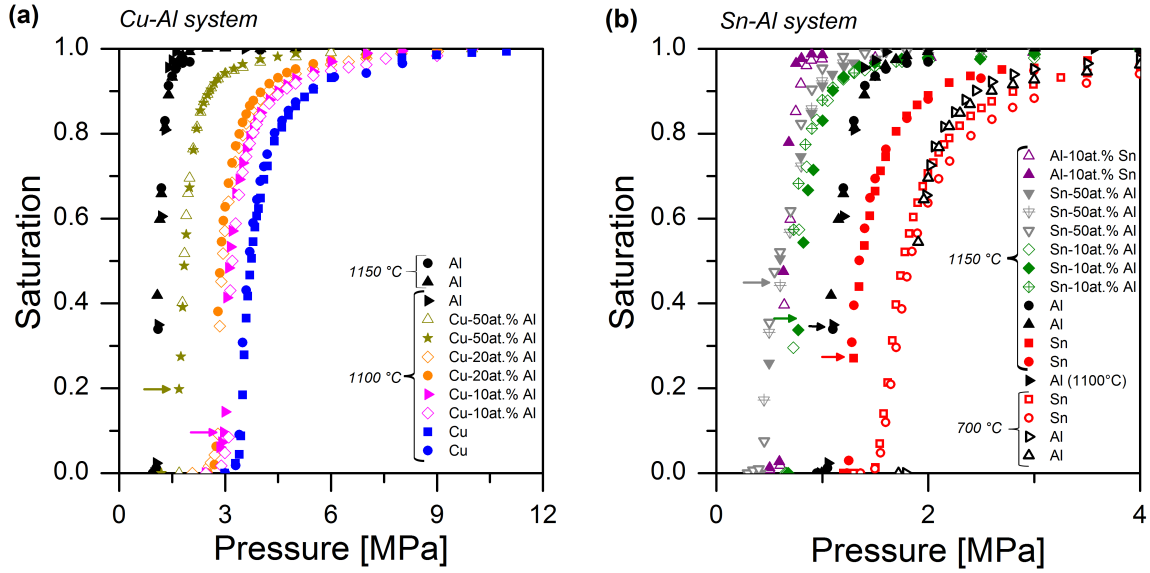

Fig. 1. Saturation curves for CIPed Al_2O_3 preforms infiltrated by (a) alloys in the Cu-Al system (Cu-50at.%Al, Cu-20at.%Al, Cu-10at.%Al and Cu) at 1100°C or (b) in the Sn-Al system (Al-10at.%Sn, Sn-50at.%Al, Sn-10at.%Al, Al and Sn) at 1150°C (and 700°C for Sn and Al) under stepwise increasing pressure. The arrows represent the final pressures applied to produce partly infiltrated composites (1.7 MPa for Cu-50at.%Al, 3 MPa for Cu-10at.%Al, 0.6 MPa for Sn-50at.%Al, 0.9 MPa for Sn-10at.%Al, 1.2 MPa for Al and 1.3 MPa for Sn).

The final published article is available at Elsevier as: A. Léger, L. Weber and A. Mortensen, "Influence of the wetting angle on capillary forces in pressure infiltration", *Acta Materialia*, Vol. 91 (2015) pp. 57-69 doi:10.1016/j.actamat.2015.03.002.

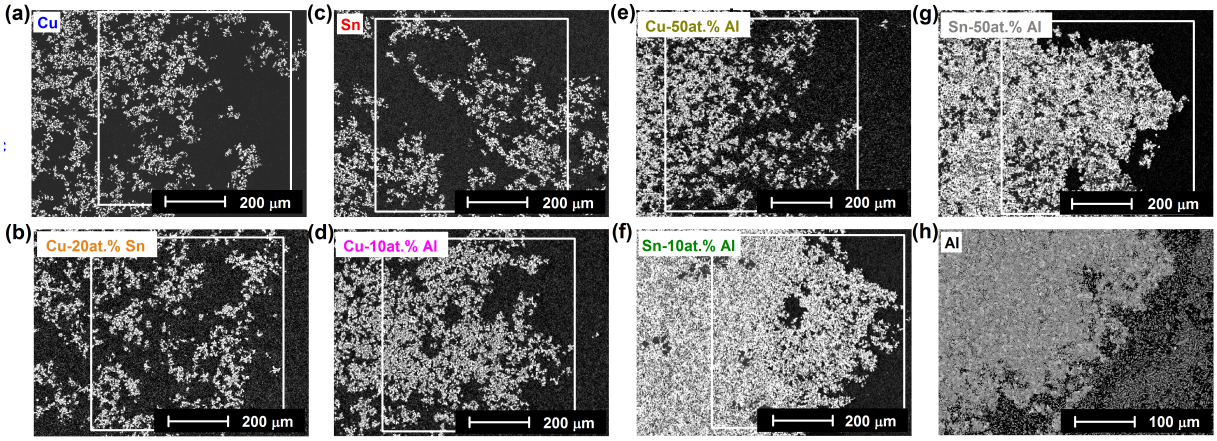

Fig. 2. Scanning electron micrographs of angular F1000 alumina partly infiltrated with (a) Cu [16], (b) Cu-20at.%Sn [17], (c) Sn, (d) Cu-10at.%Al, (e) Cu-50at.%Al, (f) Sn-10at.%Al, (g) Sn-50at.%Al and (h) Al. The white square indicates the area used to measure the fractal dimension D using the box counting method (from "ImageJ" function named "Fractal box counter"; size of the boxes: 2, 3, 4, 6, 8, 12, 16, 24, 32, 48, 64, 96, 128, 192 pixels. See Ref. [16] for more details on the fractal measurement procedure.

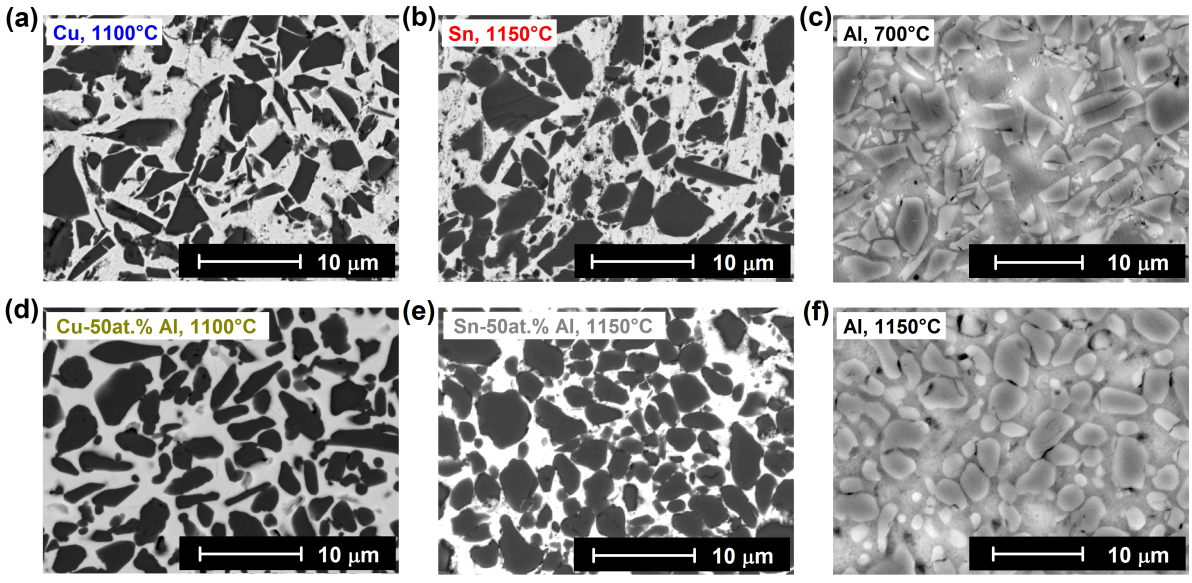

Fig. 3. SEM images of CIPed angular Al_2O_3 preforms fully infiltrated by (a) Cu, (b) Sn, (c) Al (700°C), (d) Cu-50at.%Al, (e) Sn-50at.%Al and (f) Al (1150°C).

The final published article is available at Elsevier as: A. Léger, L. Weber and A. Mortensen, "Influence of the wetting angle on capillary forces in pressure infiltration", *Acta Materialia*, Vol. 91 (2015) pp. 57-69 doi:10.1016/j.actamat.2015.03.002.

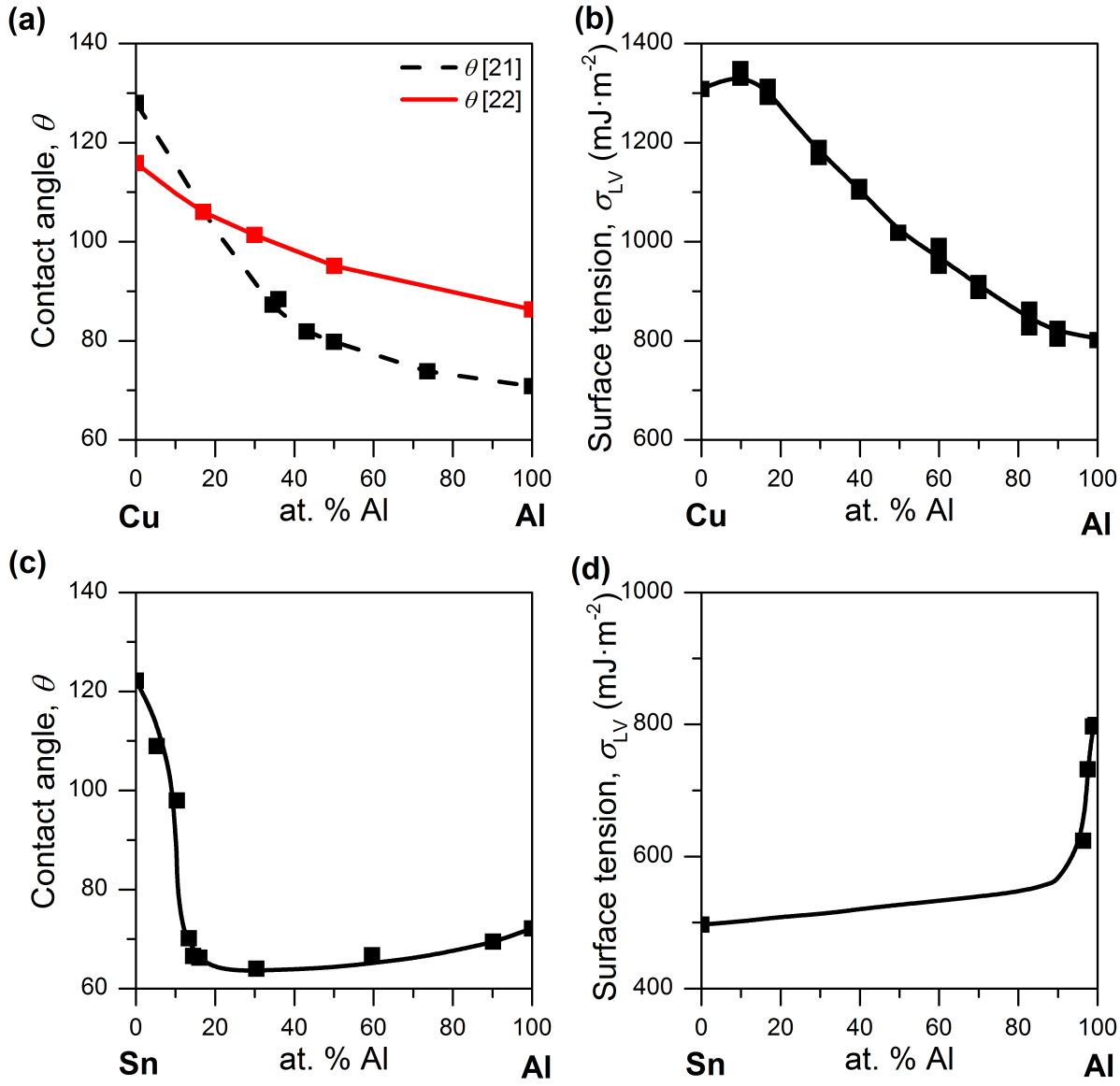

Fig. 4. (a) Contact angles on alumina from [21] measured at 1150°C and [22] at 1100°C for the crystallographic orientations $(11\bar{2}0)$ and $(1\bar{1}02)$ and (b) surface tension [23] measured at 1100°C for Cu-Al system. (c) Contact angles at 1100°C [25] and (d) surface tension for Sn-Al system obtained by extrapolation to 1150 °C of data by Goumiri *et al.* [26]; for pure tin a value of 497 mJ/m^2 is adopted, following Eq. 14 ($\sigma_{Sn} = 555.6 - 0.064\,(T\,[°C] - 232)$ mJ/m^2) of Ref. [35]. For pure aluminium a value of 798 mJ/m^2 is adopted; this is an average value of the two linear regressions from Fig. 17 of Ref [36] ($\sigma_{Al} = 890 - 0.182\,(T\,[°C] - 660)$, $\sigma_{Al} = 871 -$

The final published article is available at Elsevier as: A. Léger, L. Weber and A. Mortensen, "Influence of the wetting angle on capillary forces in pressure infiltration", *Acta Materialia*, Vol. 91 (2015) pp. 57-69 doi:10.1016/j.actamat.2015.03.002.

$0.155\ (T\ [°C] - 660)$ mJ/m^2). Square points in the plots indicate the values reported from the different sessile drop experiments.

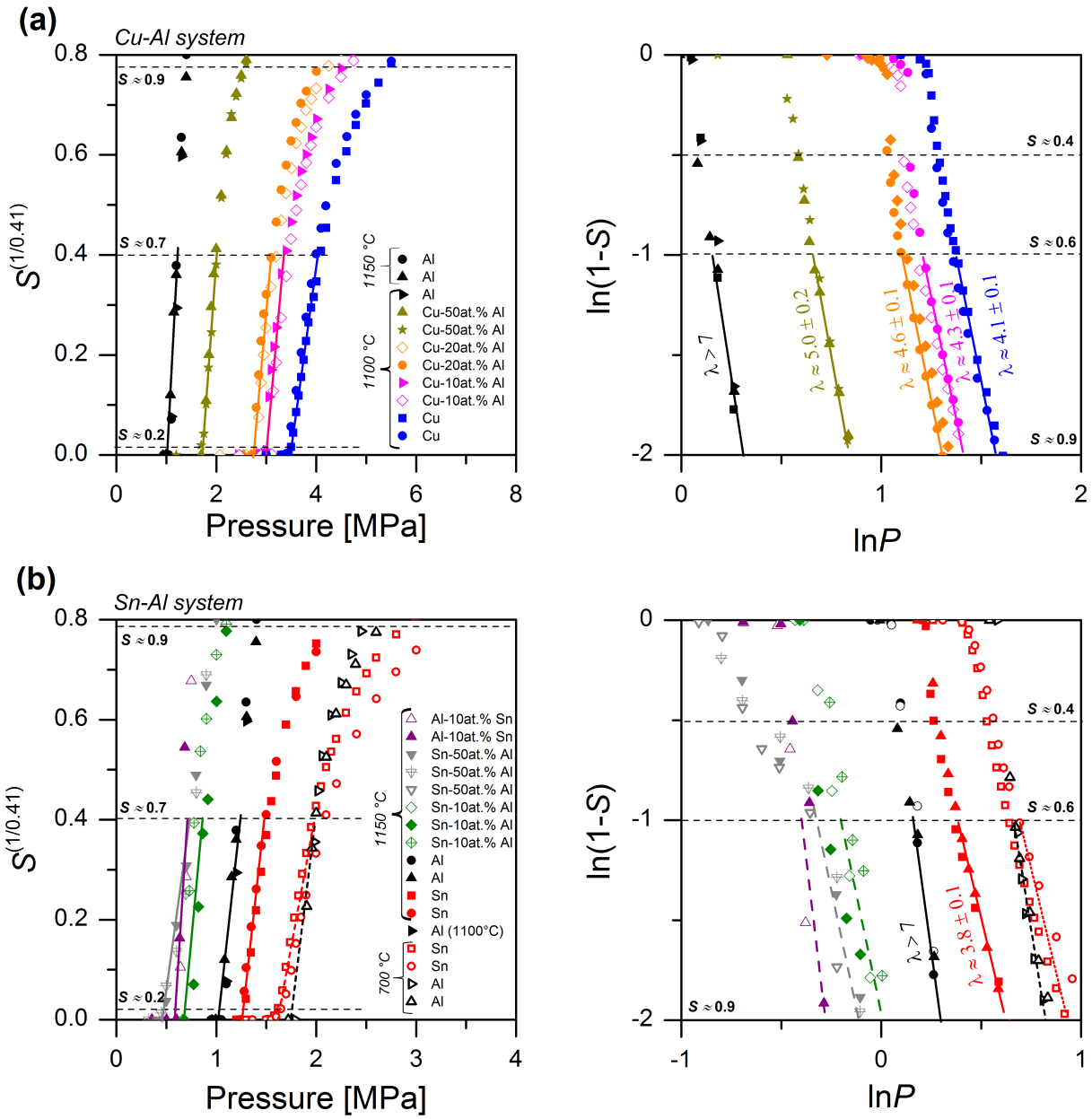

Fig. 5. Measured saturation curves for (a) Cu-Al and (b) Sn-Al, plotted (left) to test the universal scaling law given by percolation theory, Eq. 3 and (right) the semi-empirical relation proposed by Brooks and Corey, Eq. 5. The threshold pressure P_c in Eq. 3 was determined for all experiments by linear regression of data plotted as $S^{(1/0.41)}$ vs. P over the range $0.02 \leq S^{(1/0.41)} \leq 0.35$ (corresponding to $0.2 \leq S \leq 0.65$) and the pore size distribution index λ was measured in right-

hand plots by linear regression of data points over the range of -1 > ln(1-S) > -2.2 (corresponding to 0.6 ≤ S ≤ 0.9). Uncertainties in λ given above were evaluated according to Ref. [42].

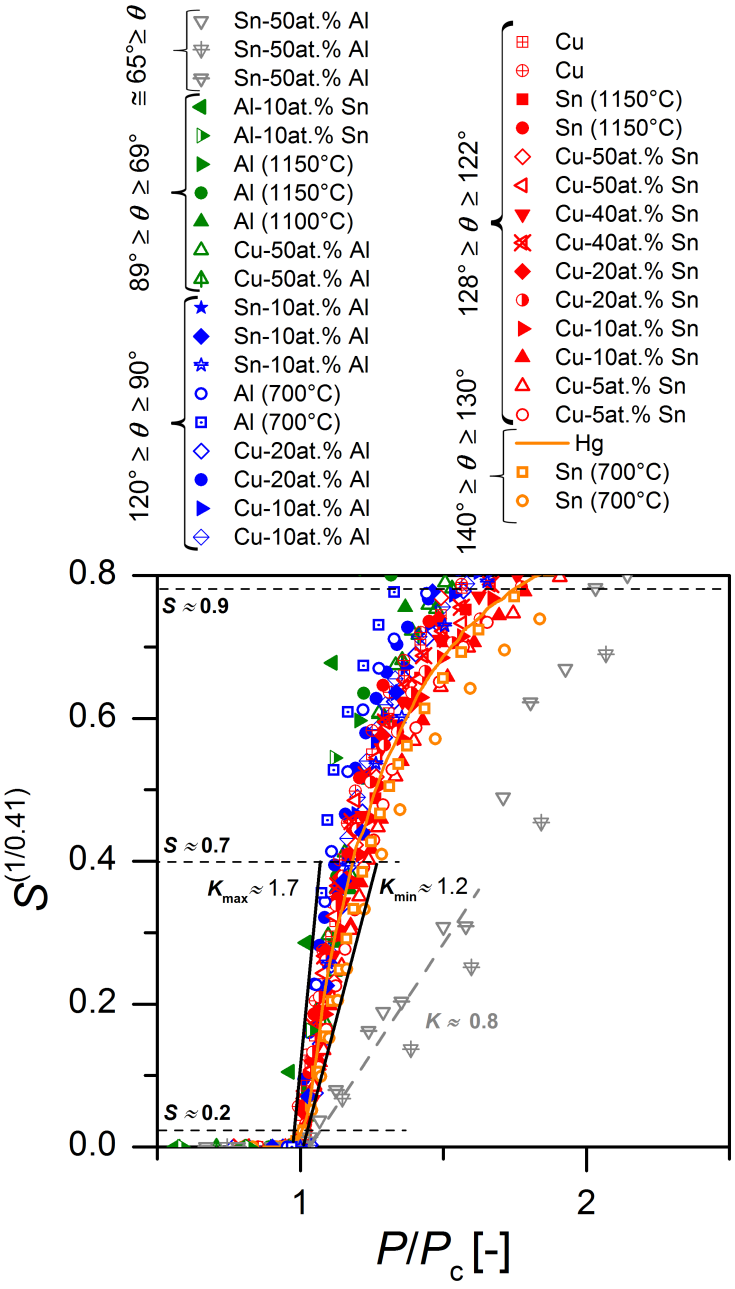

Fig. 6. Initial portion of saturation curves of all infiltration experiments in this work and in Ref. [17] replotted after division of the applied pressure P by the threshold pressure P_c for each alloy at hand.

The final published article is available at Elsevier as: A. Léger, L. Weber and A. Mortensen, "Influence of the wetting angle on capillary forces in pressure infiltration", *Acta Materialia*, Vol. 91 (2015) pp. 57-69 doi:10.1016/j.actamat.2015.03.002.

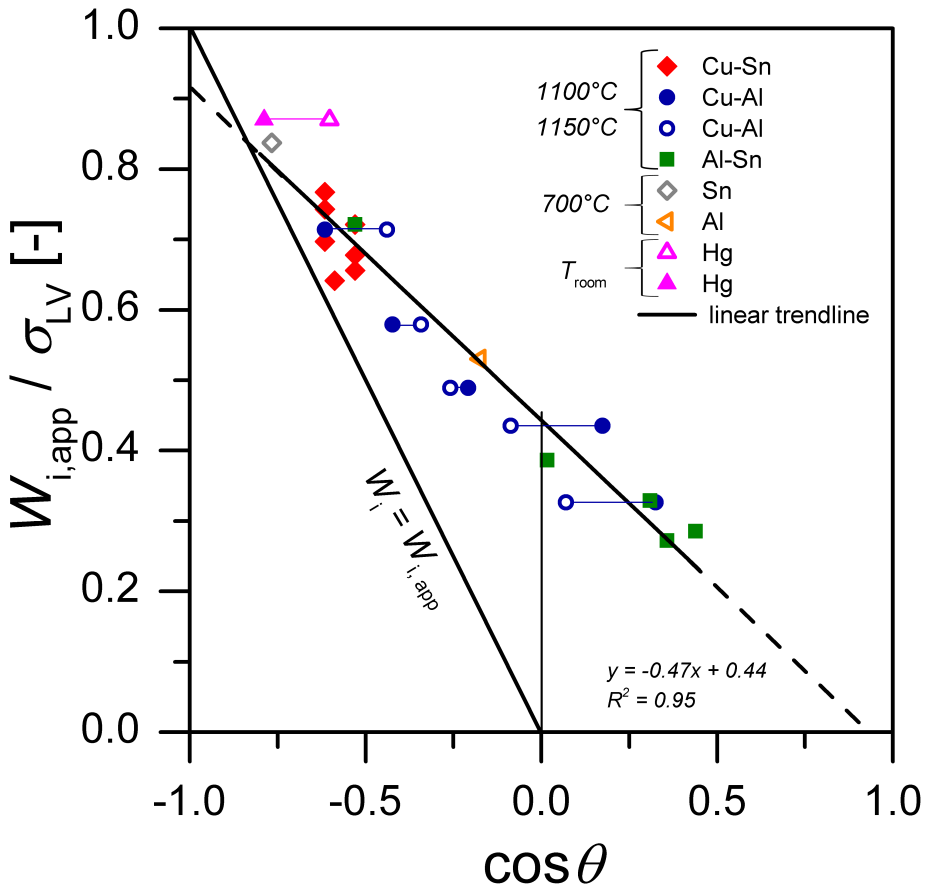

Fig. 7. Variation of $W_{i,app}/\sigma_{LV}$ (from Table 1) vs. cosθ. The trendline was obtained by linear regression assigning for all double points (having two different plausible θ) a single point, situated midway between the two.

The final published article is available at Elsevier as: A. Léger, L. Weber and A. Mortensen, "Influence of the wetting angle on capillary forces in pressure infiltration", *Acta Materialia*, Vol. 91 (2015) pp. 57-69 doi:10.1016/j.actamat.2015.03.002.

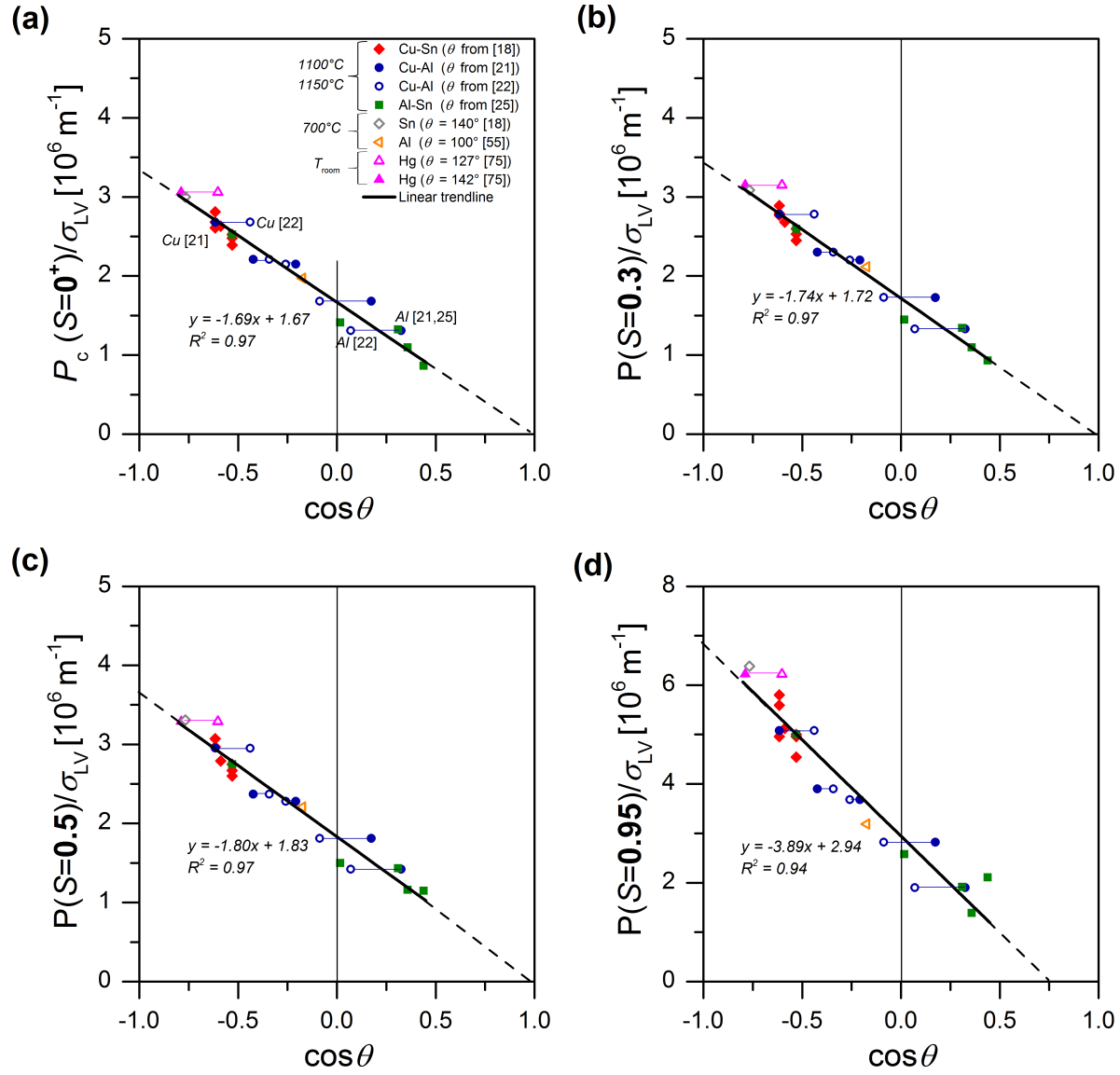

Fig. 8. Pressure P normalized by the liquid surface tension σ_{LV} plotted as the function of cosθ for the infiltration of CIPed F1000 Al_2O_3 preforms by different metals for (a) $S = 0^+$, (b) $S = 0.3$, (c) $S = 0.5$ and (d) $S = 0.95$. Values for σ_{LV} and θ are taken from Fig. 4 (a horizontal line joins values for the same system where two different plausible θ values are given in the literature; see Fig. 4). Values for Cu are from Ref. [16] and Cu-Sn from Ref. [17]. The threshold pressure P_c was determined as described in the main text. The trend line in each plot was obtained by linear regression assigning for all double points (having two different plausible θ) a single point situated midway between the two.

The final published article is available at Elsevier as: A. Léger, L. Weber and A. Mortensen, "Influence of the wetting angle on capillary forces in pressure infiltration", *Acta Materialia*, Vol. 91 (2015) pp. 57-69 doi:10.1016/j.actamat.2015.03.002.

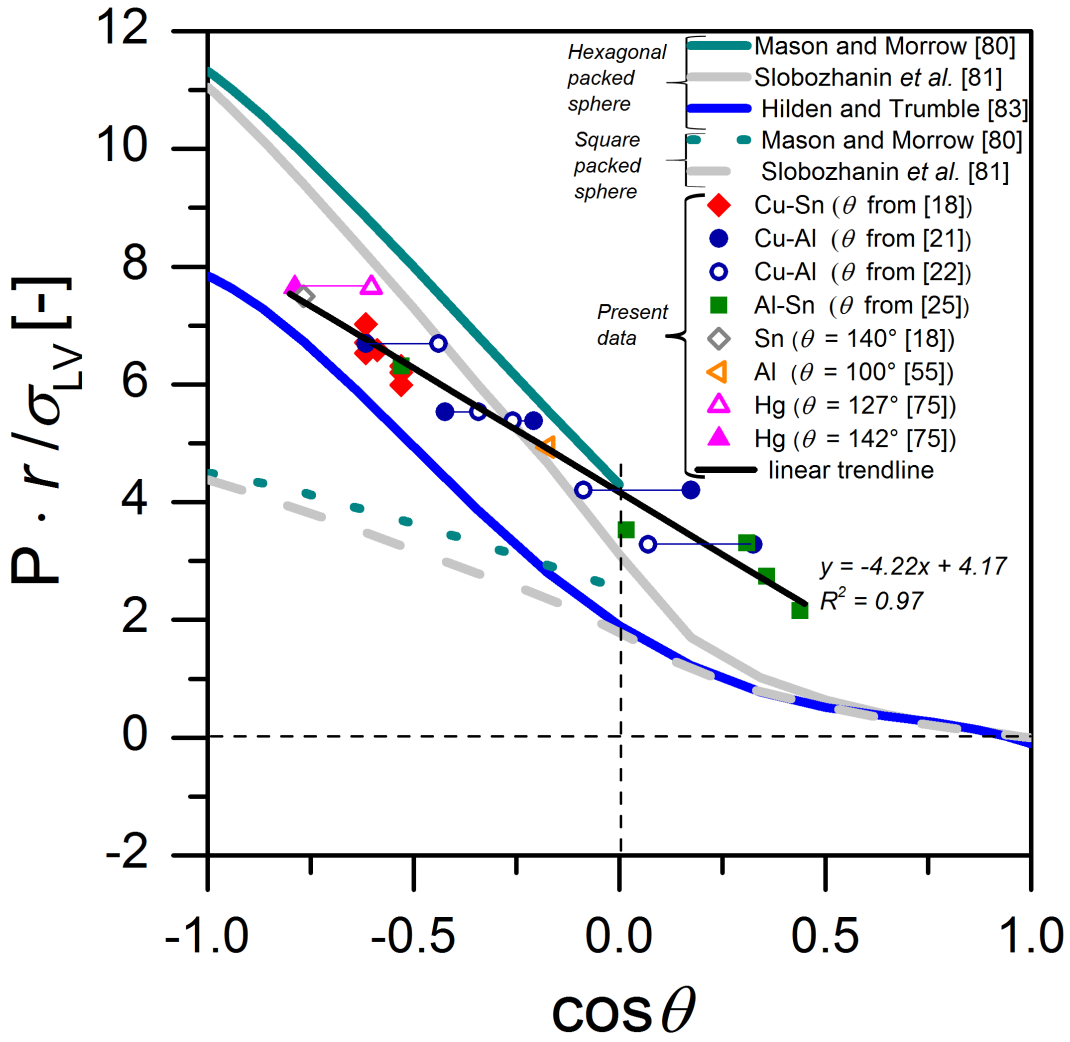

Fig. 9. Comparing plots of normalized pressure P versus cos θ for experimental data (P_c with an average r = 2.5 μm, black line) and existing models from the literature [82-83, 85]. The trendline was obtained by linear regression assigning for all double points (having two different plausible θ) a single point, situated midway between the two.